Starting characteristics of a rectangular supersonic air-intake with cowl deflection

S. Das **J. K. Prasad**
sudipdas@bitmesra.ac.in **jkprasad.1@gmail.com**
Department of Space Engineering and Rocketry
Birla Institute of Technology
Mesra, Ranchi
India

ABSTRACT

Experimental and computational investigations have been made to obtain the details of the flow field of a supersonic air-intake with different cowl deflection angles and back pressures at the exit. The flow field obtained with an inviscid computation on the basic configuration, designed for Mach 2·2, shows starting behaviour whereas computation with k-ω turbulence model and experiments indicate unstart characteristics. Both experiments and computations indicate that provision of a small angle at the cowl tip leads to start of the same intake and also improves it's performance. Results obtained with cowl deflection shows a better performance in comparison to performance achieved with a basic intake and with a bleed of 2·8%. Sustainable back pressure could be obtained through the computations made at different back pressures for different cowl deflection angles. Overall results suggest that provision of small cowl deflection angle itself leads to improvement in performance achieved in comparison to a bleed of 2·8%, even with back pressure at the exit.

NOMENCLATURE

A_t	throat area
A_c	capture area
A_e	exit area
CR	contraction ratio (A_t/A_c)
h_c	Intake capture height
L	overall length of model
m_e	mass flow rate at diffuser exit (kg/s)
m_i	capture mass flow rate (kg/s)
P	static pressure
P_b	back pressure
P_{bs}	sustainable back pressure
P_i	free stream pressure
P_{0e}	total pressure at exit
P_{0i}	total pressure of free stream
PE	pressure ratio at exit (P_b/P_i)
θ_1	first ramp angle
θ_2	second ramp angle
θ_3	first diffuser angle
θ_4	second diffuser angle
θ_c	cowl deflection angle
x	distance from leading edge
Y	distance along the height of intake
Y_{max}	maximum intake exit height
TH	ratio of throttled area at exit and throat (A_e/A_t)
FD	flow distortion
PR	pressure recovery

Paper No. 3350. Manuscript received 6 October 2008, accepted 7 September 2009.

https://doi.org/10.1017/S0001924000003626 Published online by Cambridge University Press

1.0 INTRODUCTION

Extensive studies are being done to develop air-breathing engines for aerospace application with an objective to achieve better performance during atmospheric flight. The quality and quantity of air to be delivered to the engine is achieved through a suitably designed air-intake for efficient operation at various Mach number regimes. At supersonic Mach numbers, the air-intake should diffuse the incoming atmospheric air to a desired subsonic Mach number suitable for the engine. Different methods adopted to accomplish this diffusion process are either external or internal or mixed i.e. a combination of external and internal compressions.

The performance of a mixed compression air-intake is judged by its capability to deliver the necessary mass flow to the engine with minimum total pressure loss and flow distortion. One of the major problems associated with the mixed compression intakes is the unstart process. This phenomenon will influence the mass flow rate and characteristics of the flow field inside the intake and could also affect the stability of the engine. Generally unstart of the intake is observed through expulsion of the shock system and massive spillage, leading to degraded pressure recovery and large flow distortion at the exit. The unstart of the intake could occur due to several reasons, e.g. over-contraction, variation of flight conditions, perturbations in combustor operation, back pressure, angle of attack, etc., or due to a combined effect of these factors. The presence of flow induced separation in the internal duct could also lead to unstart of the intake, generally termed as soft unstart. Interaction of the boundary layer with shock reflections and subsequent thickening of the boundary layer inside the internal duct, are believed to be the prime cause of a separation leading to a complex oscillatory flow structure and expulsion of the shock and hence the unstart of the intake.

A sketch showing the presence of the complex flow field in the intake is presented in Fig. 1. At design Mach number, the compression shock is expected to get reflected from the cowl tip. This will interact with the existing boundary layer on the ramp surface and might lead to formation of a separation zone. The strength of the reflected shock and the state of the boundary layer will be the decisive factor for the extent of separation. Various researchers have made studies for understanding the complex flow field existing inside supersonic air-intakes, especially in the region of flow interactions. In order to avoid unstart, various methods are being attempted e.g. variable geometry, spillage through wall perforations, bleeding at different locations, over speeding, fluid injection, etc. Neale and Lamb[1-4] reports experimental studies made on a combined external/internal compression intake designed at M = 2·2. Variable geometry, different bleed systems, and different diffuser shapes were adopted to overcome the starting problem.

Once the flow is separated, unsteadiness of the flow field could lead to flow instabilities inside the subsonic diffuser of air-intakes and buzz, as reported by Fisher *et al*[5] and Trapier *et al*[6-8]. Unsteady behaviour of flow in the internal duct of air-intakes at subcritical and supercritical conditions is reported by Newsome [9], Liou *et al*[10], Hsieh *et al*[11]. and Biedron *et al*[12]. Experimental studies to capture unsteady behaviour of flow in a supersonic intake is reported by Hirschen *et al*[13]. The effect of sidewall configurations on the performance of two-dimensional air-intakes operating at supersonic speed is discussed by Watanabe *et al*[14]. The occurrence of unstart phenomena of hypersonic intakes, which is different from unstart of supersonic intakes, is dealt by Tan and Guo[15], Wagner *et al*[16], Tan *et al*[17], Lanson *et al*[18], etc.

To alleviate the unstart phenomena, VanWie *et al*[19] adopted flow injection. Babinsky *et al*[20-21] demonstrated that, use of micro ramp vortex generators controls the boundary layer and leads to improvement in inlet performance. Numerical investigation to study the effect of bleed flow rate, bleed hole geometry is reported by Mizukami *et al*[22], Syberg *et al*[23] and Vivek and Mittal[24]. The effect of wall perforation on the starting of a supersonic intake is reported by Najafiyazdi *et al*[25]. Experimental and computational studies by Hermann *et al*[26] and Reinartz *et al*[27], deals with the effect of isolator length on the intake performance at supersonic Mach numbers. These methods adopted to improve the performance, need complex subsystems either to bleed or vary the duct geometry. Recent studies by Tillotson *et al*[28] and Kim[29] indicates the possibility of using a bump in the intake, which could alter the shock wave boundary-layer interaction inside the intake duct and improve the overall performance.

A small deflection of the cowl tip would lower the strength and location of the reflected shock on the ramp and could improve the downstream flow field and the performance. Adoption of small cowl bending leads to an improvement in the starting characteristics of a ramp-compression inlet at Mach 4, as reported by Kubota *et al*[30]. Alleviation of unstart and improvement in performance of mixed compression supersonic air-intake due to cowl deflection is reported by Das and Prasad[31,32]. Back pressure at the exit of the intake will also affect the existing flow field in the intake. Studies with cowl deflection and back pressure have not been investigated and reported so far, to the best of knowledge of authors.

In the present investigation a study has been made to capture the flow field inside the intake due to a small cowl angle for a typical intake geometry at different back pressures. Experiments and computations are made to capture the flow field and the performance has been estimated. The improvement in performance of the intake achieved by a conventional technique of bleed has been compared with the improvement in performance achieved with cowl deflection.

2.0 GEOMETRICAL DETAILS OF INTAKE

A rectangular mixed compression air-intake, having a design Mach number of 2·2, has been studied in the present investigation. This is similar to the configuration studied by Neale and Lamb[1]. It has a capture height (h_c) of 15mm with an aspect ratio of 1. Figure 2 shows the dimensional details of the model. The external compression is achieved through two ramps (AB and BC) having

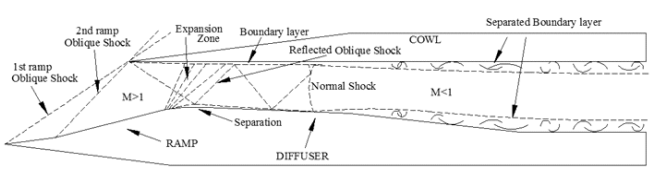


Figure 1. Details of flow field over mixed compression intake.

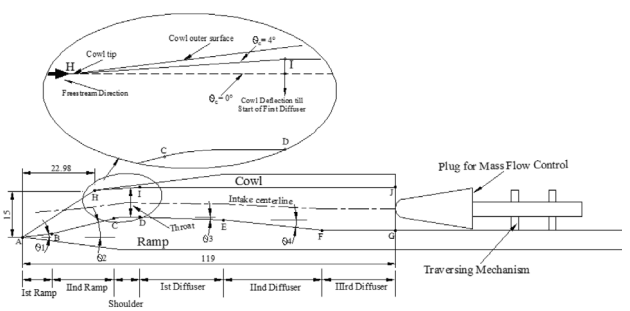


Figure 2. Dimensional details of intake model (dimensions in mm).

https://doi.org/10.1017/S0001924000003626 Published online by Cambridge University Press

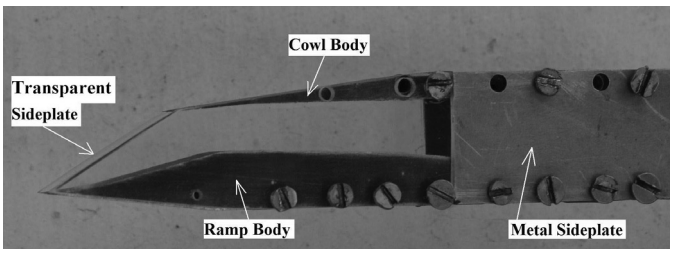
angles of $\theta_1 = 7°$ and $\theta_2 = 14°$ with respect to the free stream flow direction. After a small curved and straight portion (CD) of 8·25mm, the diffuser sections starts. The first diffuser (DE) has a turning angle of $\theta_3 = 2·3°$, whereas the second diffuser (EF) has a turning angle of $\theta_4 = 6°$ with respect to intake centerline which provides the necessary divergence. Further it is followed by a straight diffuser section (FG) till the exit. The diffuser length of the intake of Ref 1. was marginally truncated to accommodate it in the present wind-tunnel. The cowl tip (H) is positioned at a distance of 22·98mm from the ramp leading edge. The cowl was deflected about the tip H, such that it's inner surface deflects away from centerline of the intake till point I, which is almost at the same axial distance of point D. Downstream surface (IJ) is maintained parallel to the free stream direction. During the present study, the cowl deflection angle (θ_c) was varied in the range of 0° to 4° , which leads to a maximum change of about 1mm in height of the diffuser section of the intake (Refer to the enlarged view as insert). The tip of the ramp and cowl is maintained as sharp and at an angle of 7° with respect to the free stream on the external surfaces till some distance downstream. This distance is provided to minimise the disturbances due to the external surface. Further downstream it is maintained as flat. The overall length and width of the model is 119mm and 15mm respectively. This particular geometry has been used for experiments and as well for computations. During the experiments, the mass flow through the intake was varied by traversing a blunt conical plug as shown in Fig 2.

3.0 EXPERIMENTAL SETUP

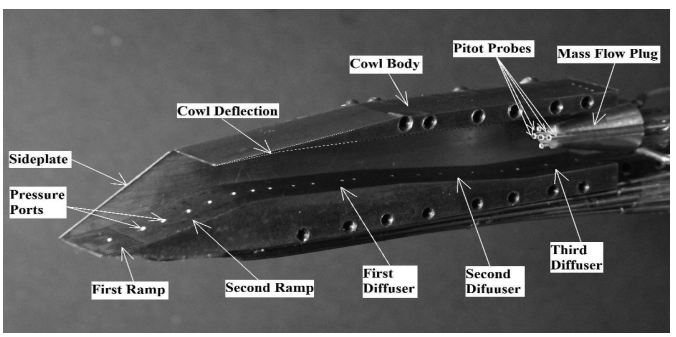
All the experiments have been performed using the Supersonic wind-tunnel at Birla Institute of Technology, Mesra, Ranchi. It is a blowdown type wind-tunnel having a rectangular test section size of 50mm × 100mm and Mach number ranging from 1·2 to 3·0. The present series of experiments have been made at a fixed Mach number of 2·2. Settling chamber pressure of about $3·5 \times 10^5 N/m^2$ was maintained which corresponds to free stream Reynolds number of $3·8 \times 10^7$ per meter. The pressure in the settling chamber is measured using a pressure transducer (Make Sensym, Model ASCX150DN). The estimated error in measurement of settling chamber pressure and static pressure is around 0·6% which corresponds to about 1% variation of Mach number in the test section.

Models were fabricated using an EDM wire cutting machine to which the dimensional details (Fig. 2) were provided in digital form, which ensured the dimensional accuracy of all the models better than 0·01mm. The models were made in modular form for ease in handling. Different models were made for flow visualisation and for pressure measurement, which are shown in Fig. 3(a,b). To capture the overall flow field, a standard schlieren flow visualisation technique was adopted. For capturing the internal flow inside the intake, the sidewalls were fabricated using Plexiglas which provided limited optical transparency. Streaks of flow on the various surfaces of intake was obtained by making use of a suitable mixture of Titanium dioxide, Oleic acid and lubricating oil. The mixture sprayed over the internal surface of the model forms streaklines on the surfaces due to the flow, which was captured using a digital camera (Model: Sony DSLR A100K).

Static pressures were measured at different locations on the ramp surface by providing pressure ports of 0·8mm diameter which were suitably connected to a 32 channel Electronic Pressure Scanner (Make: SCANCO, Model: ZOC 22B/32Px). The photograph of the model without one of the side plates presented in Fig. 3(b) exhibits 20 static pressure ports on the ramp surface. The control of scanning rate and acquisition of pressure signals along with channel number were made using NI DAQ software, LabVIEW software and PC based Data Acquisition System. The pressure scanner module was placed very close to the wind tunnel to minimise the errors due to pressure tubing. A pitot rake having five tubes was utilised to



(a) Flow visualisation model



(b) Pressure model

Figure 3. Photograph of model.

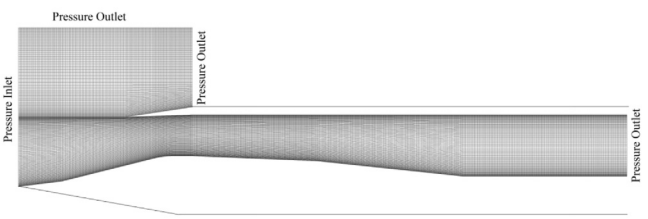
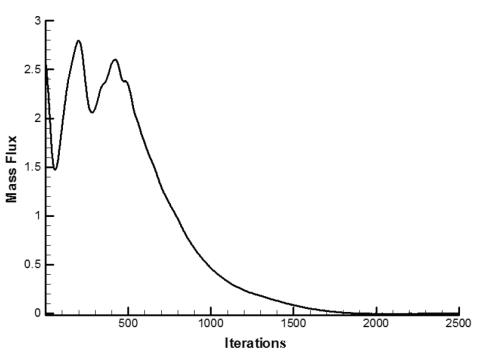
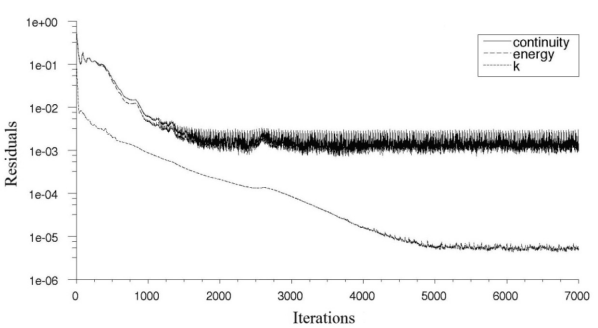


Figure 4. Grid distribution.



(a) Mass flux



(b) Continuity, energy and turbulent kinetic energy

Figure 5. Convergence history.

https://doi.org/10.1017/S0001924000003626 Published online by Cambridge University Press

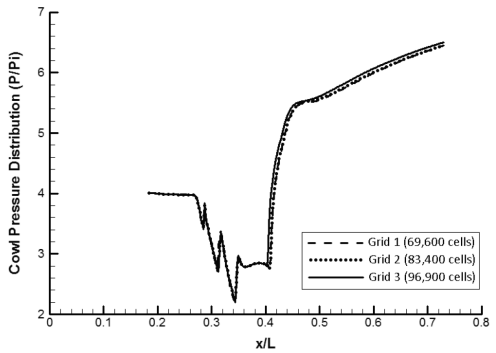


Figure 6. Pressure distribution on cowl with different grids.

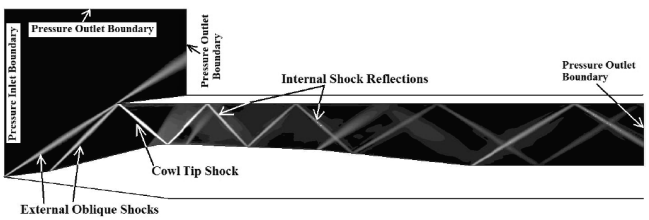


Figure 7. Numerical Schlieren from Inviscid simulation without cowl deflection.

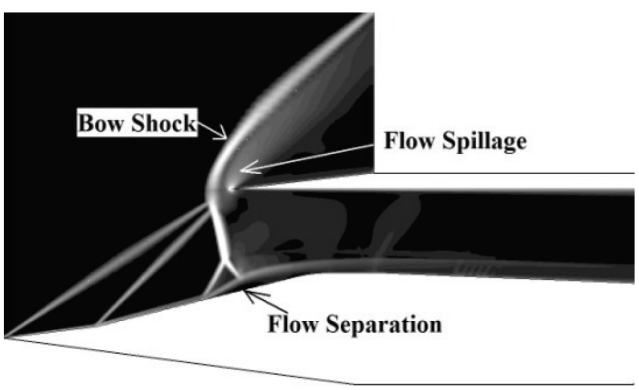


Figure 8. Numerical Schlieren from turbulent simulation for intake with $\theta_c = 0°$.

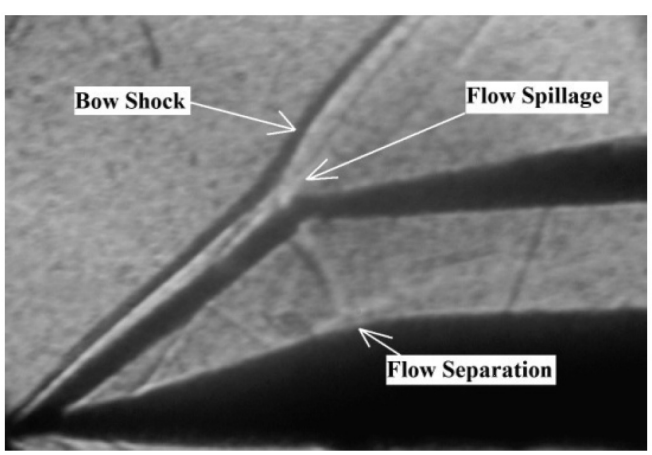


Figure 9. Schlieren photograph showing the intake flow field with $\theta_c = 0°$.

measure the total pressures at the exit of the diffuser, in the case of free flow at the exit. The Mach number at the exit for this case was estimated using the measured total pressures and static pressure at the exit. In order to throttle the intake, a blunt conical plug mounted on a traversing mechanism was used to restrict the exit area. The traversing of the plug achieved different area openings at the exit, which was estimated using the limited measurement of gap at the exit. The error involved due to the estimation of area from these measurements is estimated to be better than 3%. A stainless steel tube of 0·8mm diameter was fixed on the center of the plug which protruded 2mm. Four more tubes were fixed on the plug, such that pressures in the vertical and lateral directions could be obtained. The tips of all the tubes were maintained in the same plane. Use of the plug is expected to disturb the flow in the upstream direction, however the use of a similar method is reported in the literature.

4.0 COMPUTATIONAL TECHNIQUE

Numerical simulations were made to capture the overall flow features of the air-intake using the commercial software FLUENT. Only two-dimensional simulations have been made. Computations are performed using a finite volume technique to solve the compressible Reynolds Averaged Navier Stokes equations. An explicit coupled solver with an upwind discretisation scheme for the convective terms and second order central differencing scheme for diffusion terms in flow and transport equations was adopted. 'k-ω' turbulence model has been used, which is generally recommended for computations of complex flows involving separation and wall bounded high speed flows. Boundary conditions at inlet were specified by providing the stagnation and static pressures corresponding to a supersonic flow of Mach 2·2. A free stream turbulent intensity of 0·5% was specified at the inlet. For supersonic outflow, all the variables were extrapolated from the interior cells to the boundary. To control the mass flow, a plug has been used in the experiments, whereas in simulation a back pressure P_b, was specified at the outflow boundary. No-slip boundary conditions were enforced at all the solid walls. Computations are made for free flow (i.e. no back pressure) and with back pressures (P_b) specified by the appropriate subsonic outflow condition.

The solution domain has been restricted to the internal duct and region around the cowl tip only with appropriate boundary conditions to reduce the computational time. A typical grid distribution adopting uniformly distributed quadrilateral cells showing the overall computational domain is presented in Fig. 4. The minimum spacing near the wall in the y-direction was of the order of 0·15mm which corresponds to a y^+ value of 25. The residuals of continuity, energy and turbulent kinetic energy along with mass flux between the inflow and outflow and y^+ value on the ramp surface were monitored for solution convergence. A requirement of mass flux to drop below 1% was used as the convergence criterion. For faster convergence a 4-stage multigrid was used. Figure 5 shows typical monitors for the converged residuals and the mass flux. Computations made with three different grid refinement levels (Grid 1 (69,600 cells), Grid 2 (83,400 cells) and Grid 3 (96,900 cells)) were used to arrive at a suitable grid. Figure 6 shows the computed pressures along the inner surface of the cowl for these three grids. Based on these results and the time taken for a converged solution on a workstation, further computations have been made adopting Grid 2.

Computations have been made on the intake geometry which is similar to the experiments. Inviscid simulations are made for the intake without any cowl deflection angle i.e. $\theta_c = 0°$. Otherwise all simulations are made using k-ω turbulence model to obtain the effect of cowl deflection angles and back pressures at the exit. Turbulent simulations have been also made for $\theta_c = 0°$ and a bleed of 2·8% by providing suitable bleed holes in the vicinity of the intake throat for the purpose of intake performance comparison.

https://doi.org/10.1017/S0001924000003626 Published online by Cambridge University Press

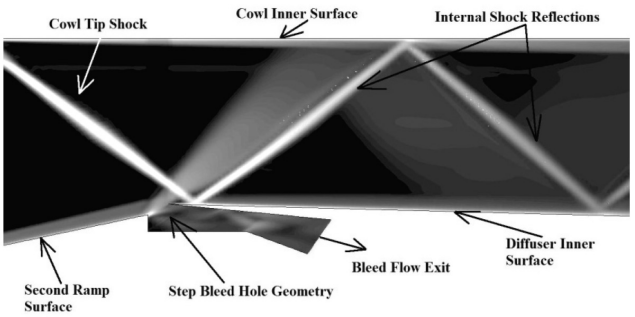


Figure 10. Numerical schlieren from turbulent simulation on intake with θ_c = 0° and step bleed (SB) of 2·8%.

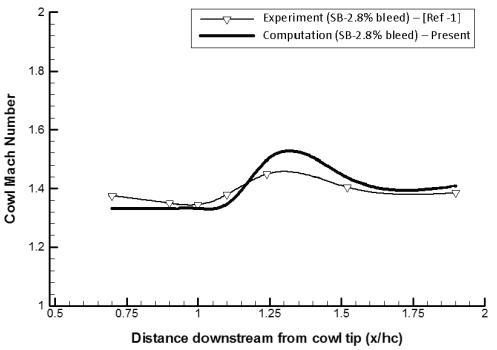


Figure 11. Comparison of computed Mach number distribution on cowl.

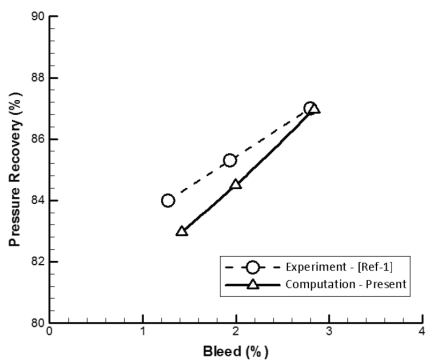


Figure 12. Comparison of computed pressure recovery.

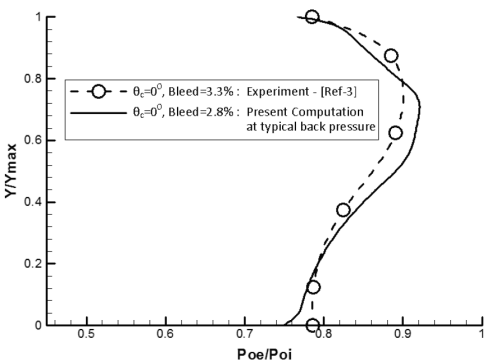
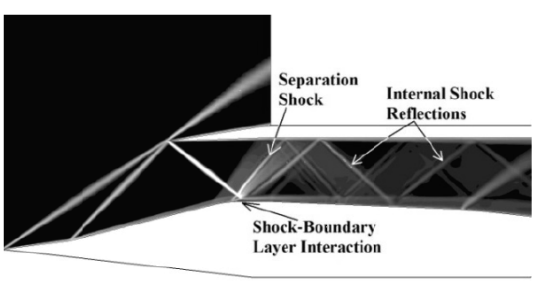
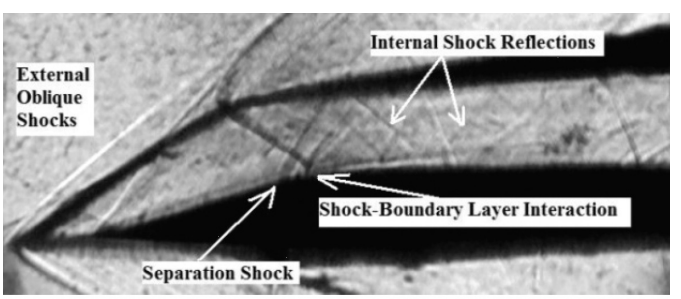


Figure 13. Comparison of total pressure distribution at the exit plane with bleed.



(a) Numerical Schlieren



(b) Schlieren (experiment)

Figure 14. Flow field with cowl deflection of 2° (θ_c = 2°).

5.0 RESULTS AND DISCUSSION

For the basic intake geometry shown in Fig. 2, the inviscid simulation has been made without any cowl deflection (θ_c = 0°). Figure 7 shows the numerical schlieren depicting the shocks at the cowl tip and subsequent reflections inside the diffuser, indicating the characteristics of the started intake. For simulations adopting a k-ω turbulence model made on the same geometry with θ_c = 0°, unstart behaviour of the intake was observed, as seen from the numerical schlieren presented in Fig. 8. Unstart of the intake could be also observed from the Schlieren photograph presented in Fig. 9, which was obtained during the present experiments with θ_c = 0°. The unstart of the intake could be due to a possible flow separation on the ramp surface which is generally termed as soft unstart[19]. Interaction of the incipient shock from the cowl tip with the boundary layer on the ramp and formation of a separation bubble near the throat etc., might lead to a thickening of the boundary layer resulting in reduction of the contraction ratio (A_i/A_c) near the throat, expulsion of the shock out of the duct and subsonic flow in the duct and hence unstart of intake.

Extensive experimental studies are reported by Neale and Lamb[1–4] with variable geometry i.e., cowl translation, different ramp angles, bleed with different geometries and mass flow rates, different subsonic diffuser configurations, etc. Some of their experimental data has been used for the purpose of validation of the present computation. Experimental data reported in Ref. 1 for the intake without any cowl deflection and with a step bleed (SB) of 2·8%, at free stream Mach number of 2·2 indicates starting behaviour of the intake. Computations have been made with Step Bleed (SB) having similar geometry and at the same location reported in Ref. 1, adopting k-ω turbulence model and suitable boundary conditions. The typical numerical schlieren showing the flow field in the vicinity of bleed hole is presented in Fig. 10, which clearly shows the starting behaviour of intake. A comparison of the computed Mach number along the cowl of intake with step bleed of 2·8% is presented in Fig. 11. Also the comparison of the

https://doi.org/10.1017/S0001924000003626 Published online by Cambridge University Press

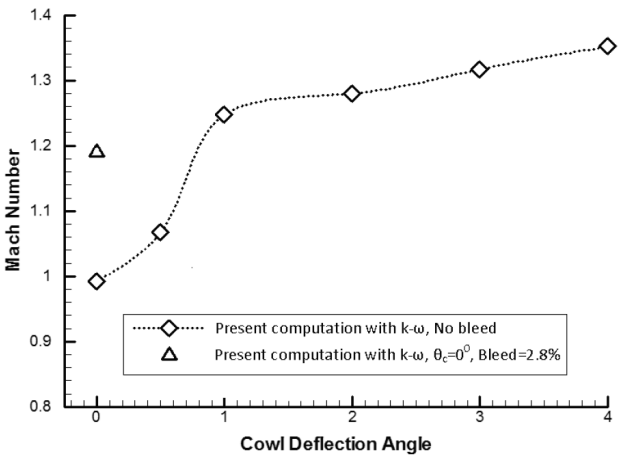
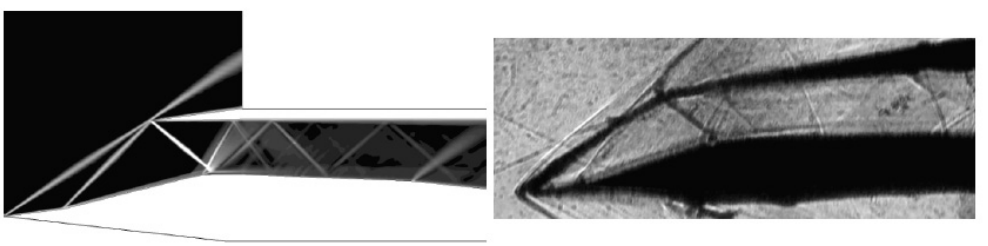


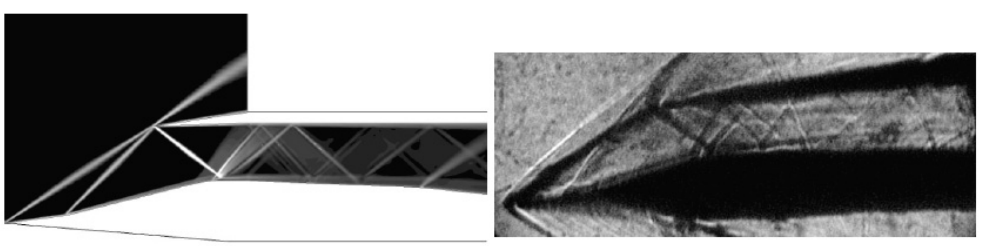
Figure 15. Computed Mach number near throat with cowl deflection.

variation of pressure recovery with step bleed at different bleed rates is presented in Fig. 12. The comparison of the measured total pressure distribution at the intake diffuser exit for the intake geometry with a bleed of 3·3% (Ref. 3) and present computed total pressures for 2·8% bleed without any cowl deflection at PE = P_b/P_i = 8 is presented in Fig. 13. A good agreement in the presence of back pressure at the exit is observed. The small differences seen could be due to the different bleed percentages. In general, the agreement between the results obtained from the present computation and the available experimental results is reasonable, which indicates the adequacy of the computational technique being adopted.

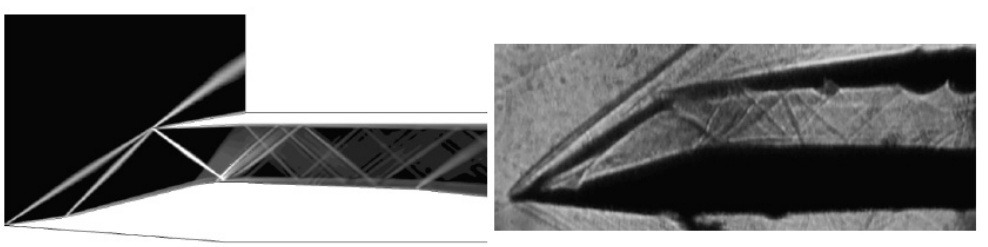
As the computation with *k*-ω turbulence model and experiments had indicated the unstart of the intake, attempts have been made to start the intake by providing a small angle to the inner surface of the cowl. This will change the location of the incident shock on the ramp and hence it will modify the flow downstream of the intake. Computations are made with a typical cowl deflection angle of 2°. The numerical schlieren for θ_c = 2° is presented in Fig. 14(a), which clearly indicates the start of the intake with the presence of a



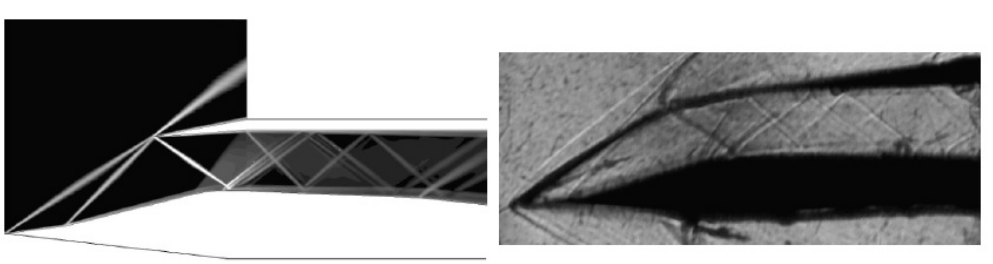
(a) θ_c=1 degree



(b) θ_c=2 degree



(c) θ_c=3 degree



(d) θ_c=4 degree

Figure 16. Behaviour of flow field at different cowl deflection angles.

https://doi.org/10.1017/S0001924000003626 Published online by Cambridge University Press

series of reflecting shock waves in the duct and the absence of spillage and flow separation which were observed for $\theta_c = 0°$ (Fig. 8). The schlieren photograph obtained for the intake with 2 degrees of cowl deflection is presented in Fig. 14(b), which indicates almost similar features as observed in the corresponding computation. The differences observed in shock angles at the ramp corners may be due to the sidewall compression. These results clearly demonstrate that provision of a small angle of the order of 2° at the cowl could start the intake.

In order to obtain the effect of cowl deflection angle, computations were made with different cowl deflection angles without any bleed. The value of Mach number near the throat area is one of the parameters which is indicative of the intake performance. Variation of Mach number at an axial location of minimum duct area (throat) with cowl deflection angle is presented in Fig. 15. Provision of a small cowl deflection angle itself indicates the start of intake. With increase in cowl deflection angle, the Mach number increases which indicates the possibility of improvement in the performance of the intake. Computation with a bleed of 2·8% but without any cowl deflection indicated the starting behaviour of the intake (Fig. 10). The value of Mach number near the throat obtained from computation with a bleed of 2·8% is also shown in the same figure, which indicates that it is comparable to the value achieved with a cowl deflection of about 1°. Studies with further increases in cowl deflection beyond 4° were not made as it will lead to substantial change in throat and exit area.

Experiments have been made with θ_c = 1°, 2°, 3° and 4° but without any bleed. Numerical and experimental schlieren are presented in Fig. 16, which clearly shows that the flow field in the internal duct near the throat improves with increase in cowl deflection angle. In general, most of the features obtained through experiments have been captured in computations. Less clarity of the schlieren photographs in experiments are due to the use of Plexiglas, which is not optically transparent. The results indicate that with increase in cowl deflection angle, the reflected shock inside the intake becomes weak and hence the strength and zone of separation would reduce.

Effect of cowl deflection angle on the ramp surface could be seen from the computed pressure distributions presented in Fig. 17. The unstart of the intake for the basic geometry (θ_c = 0°) could be observed with the presence of a steep pressure jump on the second ramp ($x/L \cong 0{\cdot}15$) suggesting the presence of a strong shock, which could be also seen in the corresponding schlieren from computation and experiments (Figs 8 and 9). Due to the provision of a small cowl deflection of 1° itself, the intake shows the starting behaviour which is seen through the presence of a series of small pressure jumps due to shock reflections inside the duct. The location of the reflected shock from the cowl tip on the ramp surface (marked with an arrow) moves downstream with increasing θ_c, and also indicates weakening of the shock strength which will lead to an increase in Mach number inside the duct. Measurement of static pressures along the centerline on the ramp surface have been made with different cowl deflection

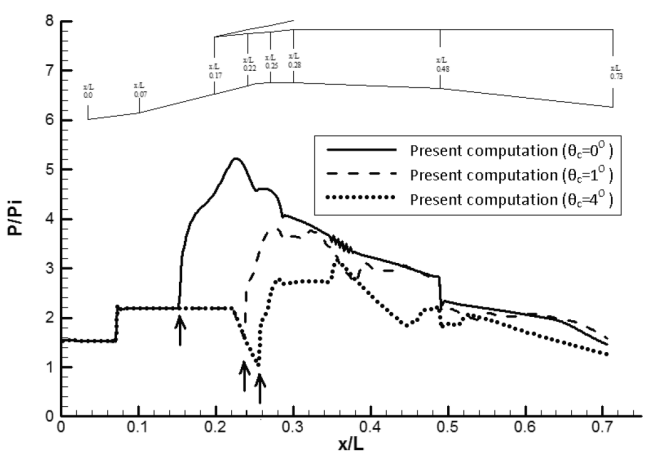


Figure 17. Effect of cowl deflection angle on pressure distribution on ramp surface.

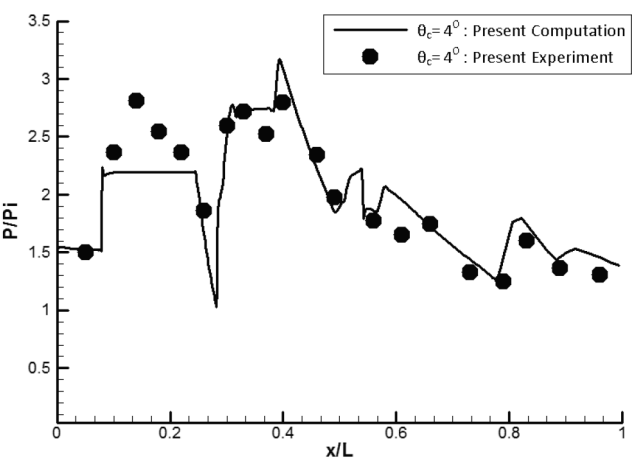


Figure 18. Comparison of computed and measured pressure distribution on ramp for θ_c = 4°.

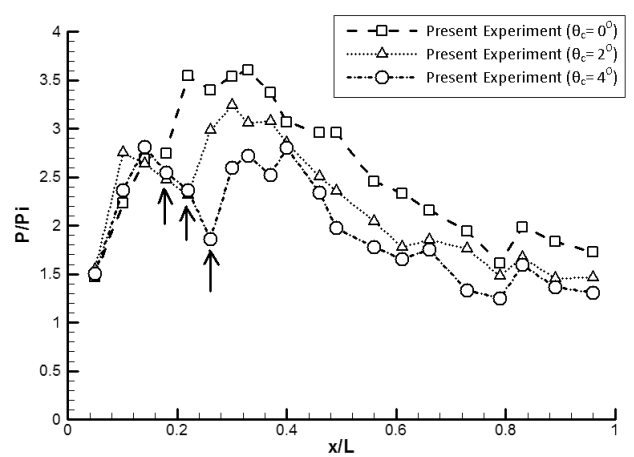


Figure 19. Effect of cowl deflection angle on measured pressure distribution on the ramp surface.

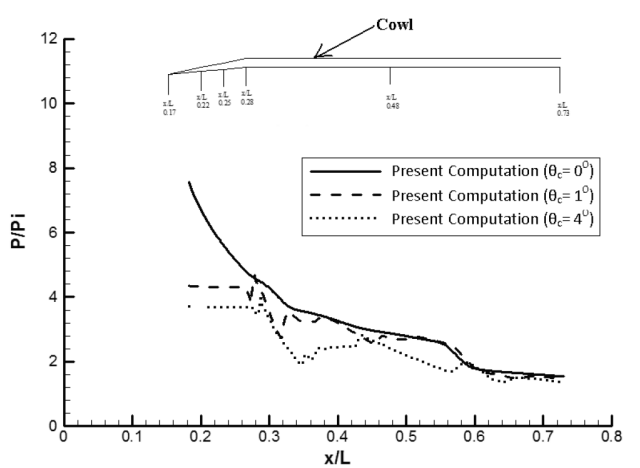


Figure 20. Effect of cowl deflection angle on computed pressure distribution on the cowl surface.

https://doi.org/10.1017/S0001924000003626 Published online by Cambridge University Press

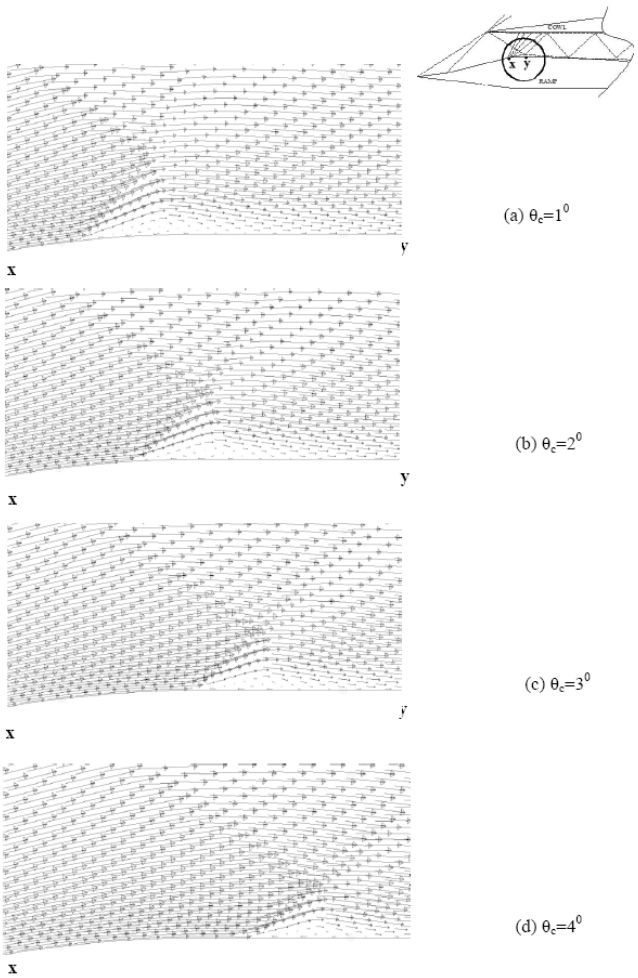


Figure 21. Velocity vectors around the interaction zone at different θ_c.

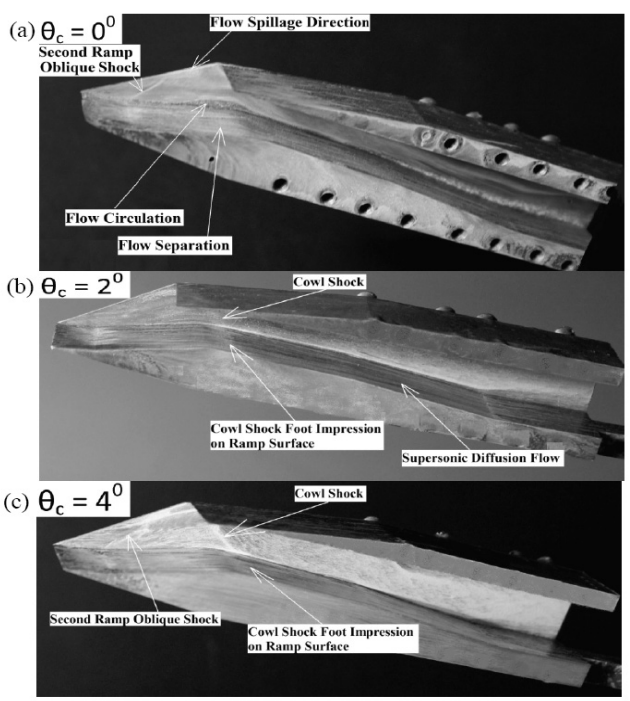


Figure 22. Surface flow pattern observed at different cowl deflection angles.

angles. Comparison of the present measured and computed pressures on the ramp surface for $\theta_c = 4°$ is presented in Fig. 18, which indicates good agreement. Differences observed in pressures on the ramp surface ($0{\cdot}08 < x/L < 0{\cdot}2$) could be attributed to the flow being three dimensional due to the presence of sidewalls in the experiments. The effect of cowl deflection angle on the measured pressure distribution on the ramp surface presented in Fig. 19, also suggests the improvement of flow inside the intake with increases in θ_c. The shock location (marked with an arrow) on the ramp surface moves downstream with increase in θ_c and seems to be in qualitative agreement with the corresponding schlieren. No measurement of pressure could be made on cowl surface due to mechanical restrictions. The pressure distribution on the inner wall of the cowl surface obtained from computation at different θ_c presented in Fig. 20, indicates that the pressure on the inner cowl surface also decreases with increases in cowl deflection angle.

The results obtained through experiments and computations clearly indicate that the flow behaviour changes with θ_c and in particular in the vicinity of throat region where strong flow interaction occurs. The behaviour of the flow field near the throat of the intake where the shock reflected from the cowl tip interacts with the boundary layer on the ramp surface, leading to formation of a separation bubble, have been visualised using the computations made at different cowl deflection angles. Velocity vectors presented in Fig. 21 for different cowl deflection angles clearly show the presence of reverse flow and a separation bubble at all cowl deflection angles. The location of the start of the separation bubble on the ramp surface moves downstream with increases in cowl deflection angle and also the size of separation bubble decreases. The presence of a separation bubble leads to thickening of the boundary layer and decreases the effective flow passage area near the throat, which could be responsible for unstart of the intake. Attempt was also made to capture these features through experiments. The surface flow pattern observed through the oil flow visualisation technique for $\theta_c = 0°$, 2° and 4° is presented in Fig. 22. At $\theta_c = 0°$, the presence of a large size separation bubble could be seen through the streak lines formed on the side wall (Fig. 22(a)). The separation zone decreases with increase in θ_c. Also the location of the shock reflected from the cowl tip could be seen at all θ_c and more clearly for $\theta_c = 4°$. The location of the shock impinging on the ramp seems to be in qualitative agreement with the pressure distribution (Fig. 19).

The performance of an intake is characterised by its mass flow, pressure recovery and uniformity of flow at the exit. Therefore measurements of total and static pressure have been made at the diffuser exit using pitot probes and a static pressure port at different cowl deflection angles. The Mach number could be calculated from these measured pressures. Average values of Mach number could be obtained from the computed results. These results presented in Fig. 23, shows similarity in behaviour of the Mach number at different θ_c obtained through experiments and computations. In general a definite gain in flow Mach number with increase in θ_c is observed for both the experiment and computation and maximum gain being at lower θ_c. This confirms that with increases in θ_c, the flow in the duct is better behaved and will lead to better performance.

The distribution of computed total pressure at the exit of the diffuser for different cowl deflection angles is presented in Fig. 24. The improvement in total pressures is observed at all θ_c, however, the improvement is maximum from $\theta_c = 0°$ to $\theta_c = 1°$ as expected. In the same figure, the computed result for intake having bleed of 2·8% and $\theta_c = 0°$ is also presented. This indicates that provision of a small θ_c leads to a pressure profile which is almost similar to a profile obtained with a bleed of 2·8%. From the pressure distributions presented in Fig. 24, the pressure recovery (PR) has been estimated using Equation (1) for various cowl deflection angles and presented in Fig. 25 with its corresponding mass flow ratio, which is defined as the ratio of mass flow at exit to the captured mass (m_e/m_i).

https://doi.org/10.1017/S0001924000003626 Published online by Cambridge University Press

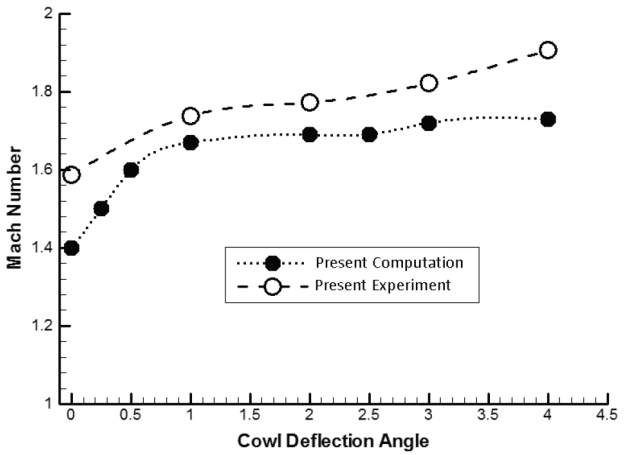


Figure 23. Variation of Mach number at intake exit with cowl deflection angles.

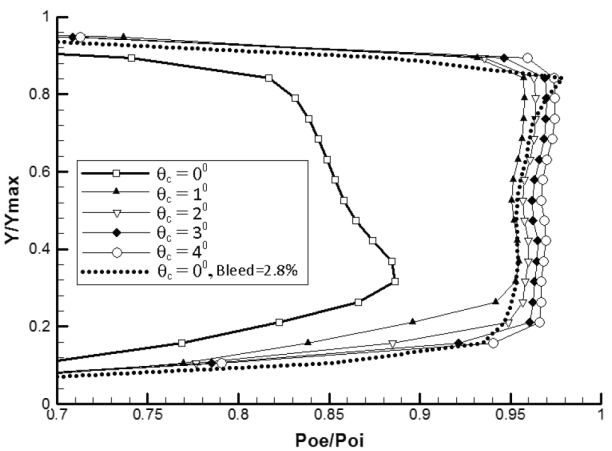


Figure 24. Computed total pressure distribution at the exit plane for different θ_c.

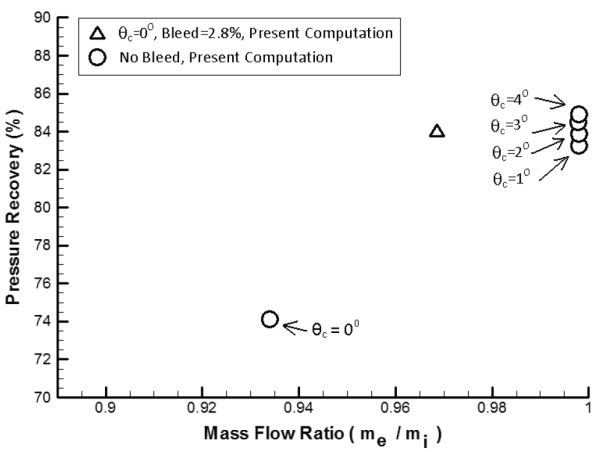


Figure 25. Intake performance for free flow exit.

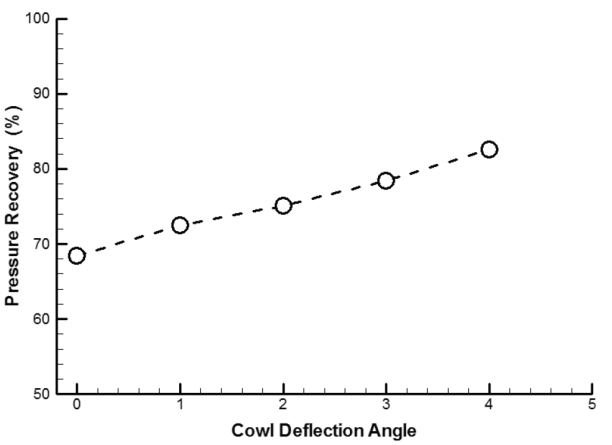


Figure 26. Pressure recovery for different cowl deflection angles obtained through experiments.

$$PR = \frac{1}{n}\sum_{i=1}^{n}\left(\frac{P_{oe}}{P_{oi}}\right)_i \quad \ldots (1)$$

Results obtained for the intake with a bleed of 2·8% and $\theta_c = 0°$, which is also presented in the same figure, shows a definite improvement in intake performance due to the adoption of cowl deflection. The pressure recovery obtained from the limited measured pitot pressures at different θ_c is presented in Fig. 26, which indicates lower pressure recovery in comparison to computations (Fig. 25). Improvement in pressure recovery with increase in cowl deflection angle is also observed in experiments.

The profile of total pressure presented in Fig. 24 clearly indicates the existence of flow non-uniformity at the exit, in particular towards the ramp and cowl surfaces. The flow distortion (FD) estimated using Equation (2) for different cowl deflection angles is presented in Fig. 27, which shows improvement in uniformity of flow at the exit with increase in cowl deflection. Here also, the flow uniformity achieved with $\theta_c = 1°$ is almost comparable with the value achieved by adopting a bleed of 2·8%.

$$FD = \left(\frac{P_{oe(\max)} - P_{oe(\min)}}{P_{oe(ave)}}\right) \quad \ldots (2)$$

The ingested air by the air-intake is compressed and supplied to an air-breathing engine at high pressures, which will vary with engine requirements. Therefore studies have been also made to capture the flow field with different back pressures. Computations at different back pressures could be made by specifying a back pressure (P_b) at the exit of the diffuser. However, in the experiments, it is achieved by traversing a blunt conical plug to restrict or throttle the exit area and hence increase the back pressure. As such, no direct relation exists, which could relate the back pressure and throttled area. The presence and location of the normal shock in the duct has been used to obtain the correspondence between the back pressure and throttled area for the purpose of comparison of the flow field behaviour. It has been observed that the flow features at PE = 7, has almost similar features obtained with TH = 1·16 and hence they are presented and discussed.

The numerical schlieren obtained for the intake with cowl deflection of $\theta_c = 4°$ at a back pressure ratio (PE = P_b/P_i) of 7, is shown in Fig. 28(a). The presence of a series of reflected oblique shocks and a normal shock is observed. The location of this normal shock, termed a terminal shock, will change with back pressure P_b. Comparison with free flow (Fig. 16(d)) indicates that the flow upstream of this normal shock seems to have almost similar behaviour. However the interaction of this shock with the boundary layers on the ramp and cowl surfaces leads to massive flow separation. The flow separation depends on the value of Mach

https://doi.org/10.1017/S0001924000003626 Published online by Cambridge University Press

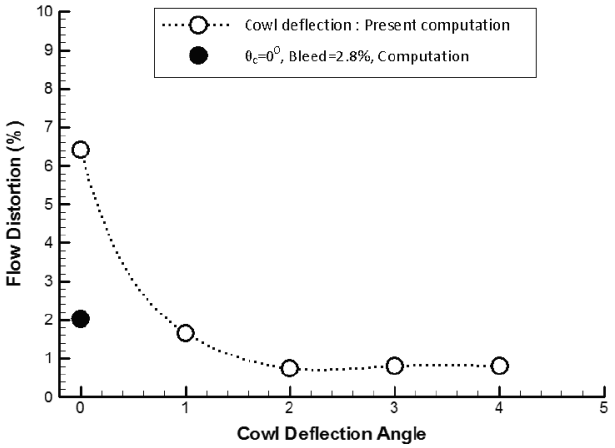
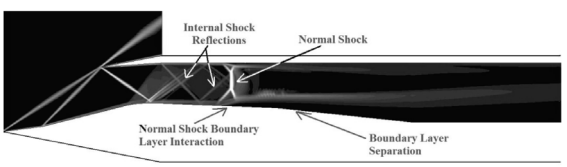
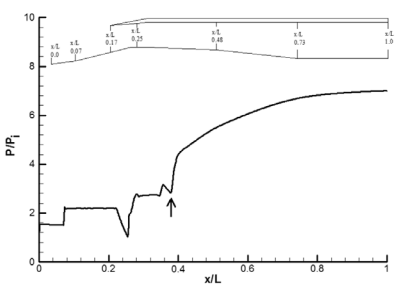


Figure 27. Flow distortion at the exit plane for various cowl deflections and for free flow exit.

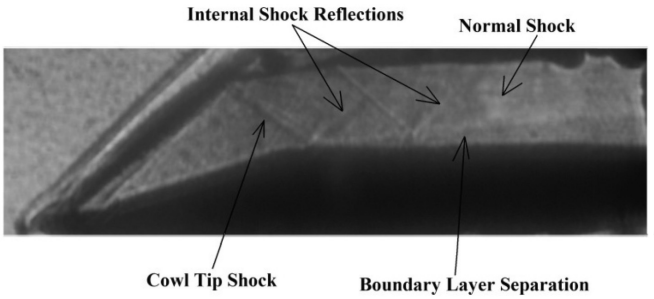


(a) Numerical Schlieren (PE = 7)

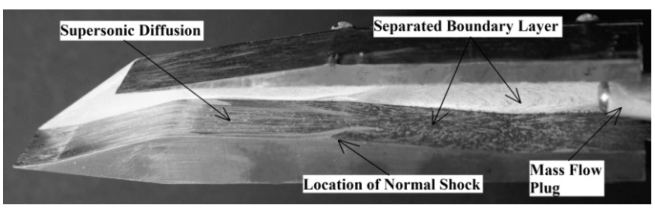


(b) Ramp pressure distribution (PE = 7)

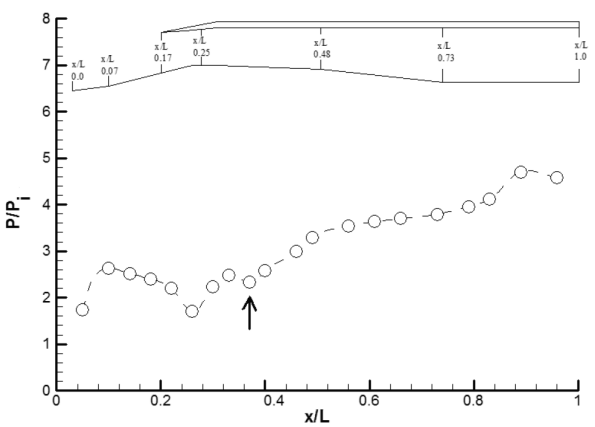
Figure 28. Computed schlieren and pressure distribution on ramp with pressurised exit (PE = 7, θ_c = 4°).



(a) Schlieren photograph (TH = 1·16)



(b) Oil flow photograph (TH = 1·16)



(c) Ramp pressure distribution (TH = 1·16)

Figure 29. Schlieren, oil flow and pressure distribution on ramp surface with throttled exit (TH = 1·16, θ_c = 4°).

number ahead of the terminal shock as reported in Ref. 33. The computed pressure distribution on the ramp surface is presented in Fig. 28(b). The presence of a normal shock could be observed through a rise in pressure at around x/L = 0·38 (marked as arrow). The behaviour of this pressure distribution up to the location of the normal shock has a similar distribution to that obtained without any back pressure (Fig. 18). The smooth rise in pressure till the exit indicates the existence of a stable and steady flow.

Schlieren and oil flow photographs obtained inside the intake with θ_c = 4° and throttle ratio (TH = A_e/A_t) of 1·16 is shown in Fig. 29(a) and (b) respectively. The presence of a weak normal shock in the internal duct is seen as a diffused region due to low transparency. The occurrence of a normal shock, separated zone and flow reversal could be seen from the oil flow photograph presented in Fig. 29(b). The measured pressure distribution on the ramp, presented in Fig. 29(c) also indicates the presence of a shock as observed by a jump in pressure at a location of x/L = 0·37 (marked as arrow). The monotonic increase of pressure downstream of the normal shock indicates the presence of a pseudo-shock in the diffuser duct as reported in Ref. 33. These results indicates that flow behaviour at PE = 7 and TH = 1·16 are almost similar.

The computed total pressure distribution at the exit of the intake with different cowl deflection angles at a back pressure of PE = 7 is presented in Fig. 30. Comparison with the pressure distribution for free flow or without enforcing any back pressure at the exit (Fig. 24), indicates different behaviour. The pressure distribution has large non-uniformity in comparison to free exit flow, which is expected. Due to back pressure, the total pressure peak is observed to be closer to the cowl surface. This may be due to different behaviour of the shock wave boundary-layer interaction existing on the ramp and cowl surfaces (Fig. 28(a)). The extent of separation on the wall surface, shape of the diffuser and the interaction will influence the flow differently on the ramp and cowl surfaces. With increases in cowl deflection angle from θ_c = 1° to θ_c = 2°, the total pressure peak has increased, however, with further increase of cowl angle to 3° and 4°, decrease in peak total pressure is observed. Comparison of results obtained for θ_c = 0° and a bleed of 2·8% and θ_c = 1° without any bleed are also shown in the same figure which indicates a good agreement.

Figure 31 shows the measured total pressures at three locations along the height of the intake for different cowl deflection angles using pitot probes fixed on the plug used for throttling. The total

https://doi.org/10.1017/S0001924000003626 Published online by Cambridge University Press

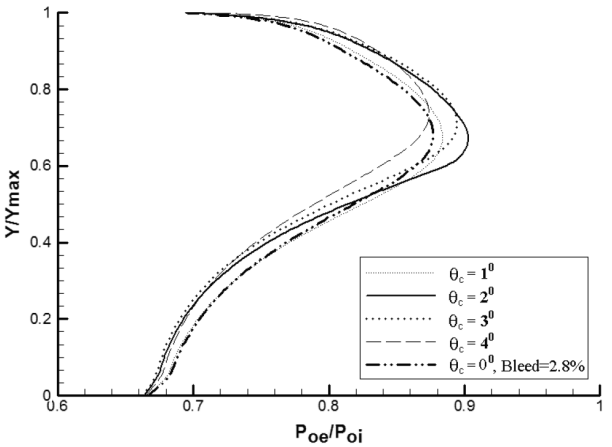


Figure 30. Computed total pressure distribution at the exit plane with pressurised exit (PE = 7) at different θ_c.

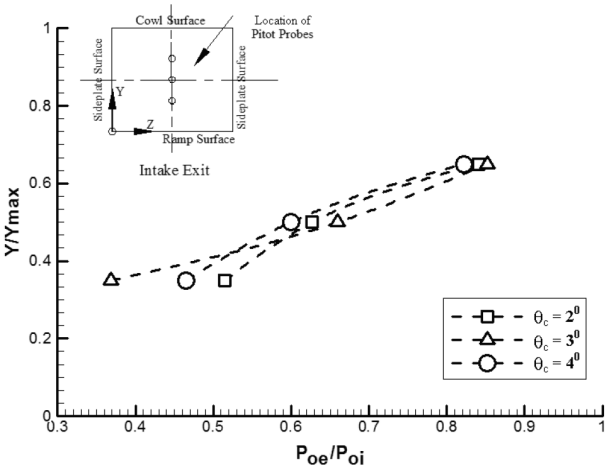


Figure 31. Measured total pressure distribution along *Y* direction at *x*/*L* = 0·85 with throttled exit (TH = 1·16) at different θ_c.

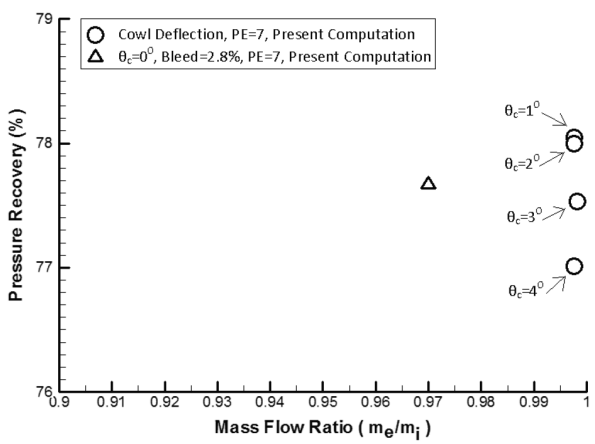


Figure 32. Intake performance at PE = 7.

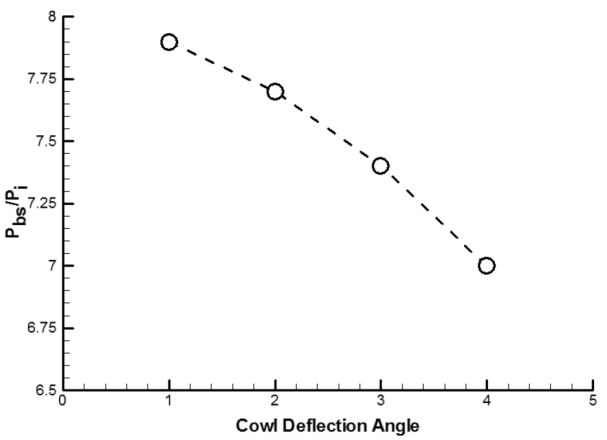


Figure 33. Variation of sustainable back pressure with cowl deflection angles.

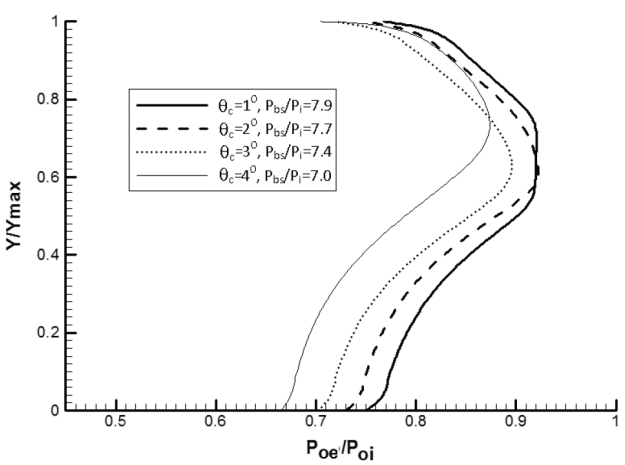


Figure 34. Computed total pressure distribution at the exit plane for different θ_c and sustainable back pressure (P_{bs}/P_i).

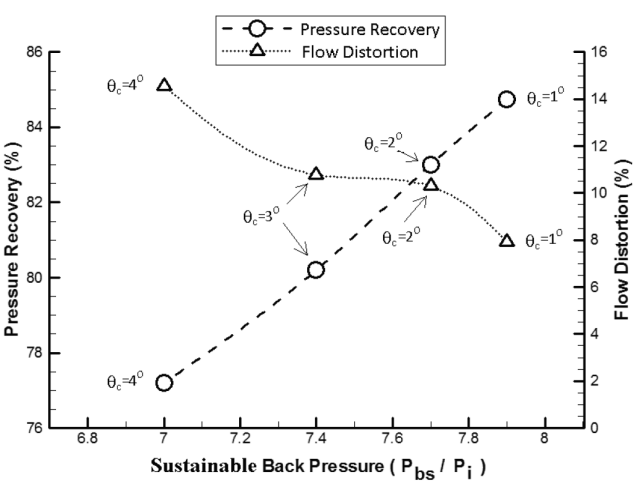


Figure 35. Behaviour of pressure recovery and flow distortion with sustainable back pressure.

https://doi.org/10.1017/S0001924000003626 Published online by Cambridge University Press

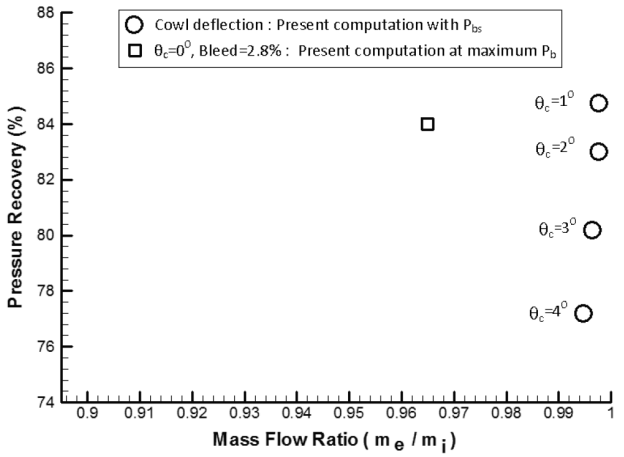


Figure 36. Performance of intake with cowl deflection.

pressure increases from ramp to cowl surface at a given θ_c. However, the behaviour with changes in θ_c is different near the ramp in comparison to the centerline and towards the cowl surface as observed in the computations.

The mass flow and pressure recovery estimated from computations at PE = 7 for different cowl deflections is presented in Fig. 32. Pressure recovery at θ_c = 1° and θ_c = 2°, is almost same. However with increase in cowl deflection to θ_c = 3° and 4°, pressure recovery decreases. Computed results with bleed of 2·8% and without any cowl deflection presented in the same figure, shows lower value of mass flow and as well lesser pressure recovery in comparison to value obtained with θ_c = 1° and 2°.

The flow field behaviour inside the intake will change with back pressure. Increasing the back pressure leads to formation of normal shock which interacts with the boundary layer. There exist the possibility that at some back pressure, the flow in the duct could become unstable and oscillation of flow could start. This could lead to buzz phenomena in the intake and may be detrimental for the intake. The limit of back pressure for the existence of a steady and stable normal shock in the intake is defined as the sustainable back pressure (P_{bs}), which has the relevance to engine. Computations were made for different cowl deflection angles and different back pressures to obtain the sustainable back pressure, through the occurrence of oscillations in the computation. The variation of the sustainable back pressure with cowl deflection angle presented in Fig. 33 indicates a decrease in sustainable back pressure with increase in θ_c. The total pressure distribution obtained at the sustainable back pressures for the corresponding cowl deflection angles is presented in Fig. 34. In general, the total pressure near the ramp surface decreases with increases in cowl deflection which is likely to be due to the presence of a normal shock in the duct. Pressure recovery (PR) has been estimated using the procedure adopted earlier for all these cases. Figure 35 shows the pressure recovery for different cowl deflection angle at it's sustainable back pressure. At lower cowl deflection angles, the sustainable back pressure and the pressure recovery is high. Sustainable back pressure and pressure recovery decreases with increase in θ_c. Similarly, the flow distortion (FD) estimate adopting the earlier procedure presented in the same figure also indicates the increase in flow distortion with increases in cowl deflection angle.

The mass flow and pressure recovery estimated for different cowl deflections at sustainable back pressures are presented in Fig. 36, and indicate that the intake has a better performance at lower values of cowl deflection. The computed result for a bleed of 2·8% without any cowl deflection is also shown in the same figure. At higher cowl deflection angles the mass flow is more in comparison to the bleed case, however the pressure recoveries are lower. In general provision of small cowl deflections of the order of 1° to 2° exhibit performance which is comparable or better than the performance achieved with bleed. The results obtained from the present series of computation and experimental investigations suggest a definite improvement in the performance of the intake in comparison to thee adoption of bleed and could be thought as an alternative to the commonly adopted method of bleed. There exists the possibility of application of combinations of cowl deflection as well as bleed to enhance the performance of the intake.

6.0 CONCLUSIONS

Computational and experimental studies have been made to obtain the flow field of a mixed compression air-intake designed for Mach 2·2 for free exit flow and with back pressure at the exit. Inviscid computations indicated start of the intake whereas computation with a *k*-ω turbulence model and experiments indicated unstart of the intake. The reason seems to be the existence of a strong shock wave – boundary-layer interaction near the throat. Studies with cowl deflection angle for free exit condition indicate starting of the intake with small values of deflection angle. The provision of cowl deflection angle reduces the strength and zone of separation near the throat region, where the strong shock wave boundary-layer interaction takes place. Increases in cowl deflection angle improves the uniformity of the flow and pressure recovery. The results indicate that a gain in performance with cowl deflection angle is comparable to the improvement obtained with the conventional method of bleed. A study with a pressurised exit indicates decreases in flow uniformity and pressure recovery with increases in deflection angle. The performance with a small cowl deflection angle, even at pressurised exit, is comparable to the value achieved with bleed. Sustainable back pressure could be obtained for different cowl deflection angle and the corresponding performance of the intake has been evaluated. The result from the present study indicates the possibility of adopting cowl deflection to improve the performance of supersonic intake.

ACKNOWLEDGEMENT

The authors sincerely thank Dr Vinay Sharma of the Department of Production Engineering, Birla Institute of Technology, Mesra, for the fabrication of models using the EDM wire cut machine. Support extended by faculty and staff of the Department of Space Engineering and Rocketry is sincerely acknowledged. We sincerely thank the reviewers for their constructive comments which were very useful for modification of this article.

REFERENCES:

1. NEALE, M.C. and LAMB, P.S. Tests with a variable ramp intake having combined external /internal compression, and a design Mach number of 2.2, Aeronautical Research Council – CP – 805, August 1962.
2. NEALE, M.C. and LAMB, P.S. Further tests with a variable ramp intake having a design Mach number of 2·2, Aeronautical Research Council C P No. 826, February 1963.
3. NEALE, M.C. and LAMB, P.S. More tests with a variable ramp intake having a Design Mach Number of 2·2, Aeronautical Research Council – CP – 938, November 1963.
4. NEALE, M.C. and LAMB, P.S. Some tests with a variable ramp intake having sidewall compression and a design Mach number of 2.2, Aeronautical Research Council, CP, 936.
5. FISHER, S.A., NEALE, M.C and BROOKS, A.J. On the sub-critical stability of variable ramp Intakes at Mach numbers Around 2, Aeronautical Research Council, Reports and Memoranda No 3711, 1972.
6. TRAPIER, S., DUVEAU, P. and DECK, S. Experimental study of supersonic Inlet buzz, *AIAA J*, October 2006, **44**, (10), pp 2354-2365.

https://doi.org/10.1017/S0001924000003626 Published online by Cambridge University Press

7. TRAPIER, S., DECK, S and DUVEAU, P. Delayed detached-eddy simulation and analysis of supersonic inlet buzz, *AIAA J*, January 2008, **46**, (1), pp 118-131.
8. TRAPIER, S., DECK, S., DUVEAU, P. and SAGAUT, P. Time-frequency analysis and detection of supersonic Inlet buzz, *AIAA J*, September 2007, **45**, (9), pp 2273-2284.
9. NEWSOME, R.W. Numerical simulation of near-critical and unsteady, subcritical inlet flow, *AIAA J*, October 1984, **22**, (10), pp 1375-1379.
10. LIOU, M.S., HANKEY, W.L and MACE, J.L. Numerical simulation of a supercritical inlet flow, AIAA, 1985, 1214.
11. HSIEH, T., WARDLAW, A.B., COLLINS, P and COAKLEY, T. Numerical investigation of unsteady inlet flowfields, *AIAA J*, January 1987, **25**, (1), pp 75-81.
12. BIEDRON, R.T. and ADAMSON, T.C. Unsteady flow in a supercritical supersonic diffuser, *AIAA J*, November 1988, **26**, (11), pp 1336-1345.
13. HIRSCHEN, C., HERRMANN, D and GULHAN, A. Experimental investigations of the performance and unsteady behaviour of a supersonic Intake, *J Propulsion and Power*, May-June 2007, **23**, (3), pp 566-574.
14. WATANABE, Y., MURAKAMI, A and FUJIWARA, H. Effect of Sidewall configurations on the aerodynamic performance of supersonic air-intake, AIAA 2002-3777.
15. TAN, H. and GUO, R. Experimental study of the unstable-unstarted condition of a hypersonic inlet at Mach 6, *J Propulsion and Power*, July-August 2007, (23), **4**, pp 783-788.
16. WAGNER, J.L., YUCEIL, K.B., VALDIVIA, A., CLEMENS, N.T. and DOLLING, D.S. Experimental investigation of unstart in an inlet/isolator model in Mach 5 Flow, *AIAA J*, June 2009, **47**, (6), pp 1528-1542.
17. TAN, H., SUN, S. and YIN, Z. Oscillatory flows of rectangular hypersonic inlet unstart caused by downstream mass-flow choking, *J Propulsion and Power*, January-February 2009, **25**, (1), pp 138-147.
18. LANSON, F and STOLLERY, J.L. Some hypersonic intake studies, *Aeronaut J*, March 2006, **110**, (1105), pp 145-156.
19. VAN WIE, D.M., KWOK, F.T and WALSH, R.F. Starting characteristics of supersonic inlets, AIAA Paper 96-2914.
20. BABINSKY, H. and OGAWA, H. SBLI control for wings and inlets, *Shock waves*, 2008, **18**, pp 89-96.
21. BABINSKY, H. Understanding Micro-ramp control of supersonic shock wave boundary-layer interactions, USAF Technical Report, AFRL-SR-AR-TR-08-0074, January 2008.
22. MIZUKAMI, M. and SAUNDERS, J.D. Parametrics on 2D Navier-Stokes analysis of a Mach 2.68 rectangular bifurcated mixed compression inlet, AIAA 95-2755, 1995.
23. SYBERG, J and KONESEK, J.L. Bleed system design technology for supersonic inlets, *J Aircr*, July 1973, **10**, (7), pp 407-413.
24. VIVEK, P and MITTAL, S. Buzz instability in a mixed-compression air intake, Technical Notes, *J Propulsion and Power*, May-June 2009, **25**, (3), pp 819-822.
25. NAJAFIYAZDI, A., TAHIR, R and TIMOFEEV, E.V. Analytical and numerical study of flow starting in supersonic inlets by mass spillage, AIAA 2007-5072, July 2007.
26. HERRMANN, C.D and KOSCHEL, W.W. Experimental investigation of the internal compression of a hypersonic intake, AIAA-2002-4130.
27. REINARTZ, B.U., HERMANN, C.D., BALLMANN, J. and KOSCHEL, W.W. Aerodynamic performance analysis of a hypersonic inlet isolator using computation and experiment, *J Propulsion and Power*, September-October 2003, **19**, (5), pp 868-875.
28. TILLOTSON, B.J., LOTH, E., DUTTON, J.C., MACE, J. and HAEFFELE, B. Experimental study of a Mach 3 bump-compression flowfield, *J Propulsion and Power*, May-June 2009, **25**, 3, pp 545-554.
29. KIM, S.D. Aerodynamic design of a supersonic Inlet with a parametric bump, *J Aircr*, January-February 2009, **46**, (1), pp 198-202.
30. KUBOTA, S., TANI, K. and MASUYA, G. Aerodynamic performances of a combined cycle inlet, *J Propulsion and Power*, July-August 2006, **22**, (4), pp 900-904.
31. DAS, S. and PRASAD, J.K. Flow field investigation of a rectangular supersonic air-intake with cowl bending, *J Aerospace Sciences and Technologies*, May 2009, **61**, (2), pp 312-324.
32. DAS, S. and PRASAD, J.K. Effect of cowl deflection angle in a supersonic air-intake, *Defence Science J*, March 2009, **59**, (2), pp 99-105.
33. MATSUO, K., MIYAZATO, Y. and KIM, H.D. Shock train and pseudo-shock phenomena in internal gas flows, *Progress in Aerospace Sciences*, 1999, **35**, pp 33-100.

https://doi.org/10.1017/S0001924000003626 Published online by Cambridge University Press